Journal of Systems Engineering and Electronics
Vol. 31, No. 3, June 2020, pp.602 – 611

Autonomous optical navigation of Mars probe aided by one-way Doppler measurements in capture stage

ZHANG Zhibin[1,2], JI Haibo[1,*], and YANG Jie[2]

1. School of Information and Technology, University of Science and Technology of China, Hefei 230026, China;
2. State Key Laboratory of Astronautics Dynamics, Xi'an Satellite Control Center, Xi'an 710043, China

Abstract: The optical navigation errors of Mars probe in the capture stage depend closely on which targets are selected to be observed in the Mars system. As for this problem, an integrated navigation scheme is proposed wherein the optical observation is aided by one-way Doppler measurements. The errors are then analyzed respectively for the optical observation and one-way Doppler measurements. The real-time calculating scheme which exploits the extended Kalman filter (EKF) framework is designed for the integrated navigation. The simulation tests demonstrate that the errors of optical navigation, which select the Mars moon as the observation target, are relatively smaller than those in the Mars-orientation optical navigation case. On one hand, the integrated navigation errors do not depend on the selecting pattern of optical observation targets. On the other hand, the integrated navigation errors are significantly reduced as compared with those in the optical-alone autonomous navigation mode.

Keywords: Mars probe, autonomous navigation, one-way Doppler measurement, optical observation, capture stage.

DOI: 10.23919/JSEE.2020.000036

1. Introduction

In Mars exploration missions, several problems should be considered, including very faraway distance, long travel interval, low data transmission rate and unknown environment in deep space. Simultaneously, the TT & C system, namely tracking, telemetry and command, on the Earth has the limited capacity in the aspects of real-time navigation and emergency handing. Therefore, from the 1960s, researchers have been focusing on the autonomous navigation methods, and abundant theory studies have been carried on [1 – 12]. Since 1990s, 16 launching missions of Mars probe have been implemented. Among them, six missions failed and five of them were due to navigation problems. In 1996 and 2011 respectively, Russian Mars 96 and Phobos-Grunt missions failed as the result of the interruption of the radio navigation in the earth-escaping stage. In 1992, American Mars Observer impacted into the Mars in the capture stage and similarly, the failure was caused by missing the radio navigation. In 1998, American Mars Climate Orbiter cracked up in the Earth-to-Mars transferring stage because of the failure on the integrated navigation. In 1999, Japan Hope Mars Probe failed to pass the Mars in the capture stage because of the low precision of the radio navigation. Therefore, the autonomous navigation in deep space is vital to guarantee the success of Mars exploration missions. At present, the autonomous navigation and orbit control based on optical measurement technologies have been widely utilized in lots of missions [13 – 19]. In May 1971, the Mars probe of American Mariner 9 firstly began to verify the optical autonomous navigation. On 24th Oct. 1998, American Deep Space 1 implemented this technology for the first time in the cruise phase. In 2003, American Mars Exploration Rover successfully applied the optical autonomous navigation in the Mars landing mission for the first time. In the capture stage, the probe travels into the Mars' gravitation range. Most of the failed missions occurred in this stage, which is mainly caused by the fact that the capture procedure lasts only 50 min. During such a short time span, the communication interruption cannot be accepted in any way. However, the delay of two-way radio communication between the ground stations and Mars probe is as long as 24.4 min. Consequently, the precision, reliability and real-time performance of the autonomous navigation become critical to the capture stage. In order to achieve the maneuver capture in this stage, the maximum position errors of the optical autonomous navigation need to be less than 120 km. At present, the autonomous optical navigation errors of most Mars probes in the cruise phase are about the magnitude of dozens of kilometers. And in the capture stage, it is no more than 10 km [20 – 22].

The optical navigation in deep space exploration missions focuses on utilizing the optical sensors to image the

Manuscript received May 21, 2019.
*Corresponding author.
This work was supported by the National Natural Science Foundation of China (61273090).

target body and then makes use of some image processing algorithms to obtain its position information. Thus, the optical sensors can provide high-precision orientation parameters. However, the optical-alone autonomous navigation is usually hard to satisfy for harsh engineering applications. First, the navigation accuracy is closely related to high-precision optical sensors which may bring tremendous costs into the design scheme. Second, some unknown faults may occur on the optical sensors of the Mars probe during the long-journey flight. Thus the multi-sensor fusing navigation has become the main solution to attacking the high-precision and reliability problems. For these considerations, the autonomous navigation filter often exploits the above orientation parameters and some aided measurements from other sensors to estimate the position and velocity of the Mars probe. The aided measurement sources usually include X-ray pulsars [23 – 25], Einstein shift [26,27], and starlight refraction measurements [28 – 32]. Liu [33] proposed an integrated navigation method based on observing the X-ray pulsars and planetoids by turns. The results indicated that multiple observations could achieve higher navigation precision than that in the single observation case. Liu [34] also proposed an integrated navigation method based on utilizing the Einstein shift and optical measurements. Based on the optical observation of the Mars and the Phobos, Ming [35] utilized the angles between the Sun and stars as measurements and implemented the autonomous navigation in the capture stage. However, the autonomous navigation methods above are mainly based on the observation of three targets in the Mars system and other observations are astronomical navigation sources. These observation sources are themselves unstable, and even their relating sensor measurement technology is not reliable in the present period. Besides, observing multiple targets simultaneously always makes the optical sensors inconvenient in the navigation implementation. Generally, different sensors must be installed on each side of the Mars probe in order to fulfill the multi-target observation tasks at the same time. Even for the single optical sensor on the Mars probe, continuous attitude maneuvering has also to be implemented to enlarge its field of view for the same end. In the cruise phase of the Mars probe, Zhang [36] concluded that the navigation errors depend closely on selecting which planetoids to be observed and determining the optimal imaging sequence of planetoids. The above results adequately show that the selective strategy of optical observation targets is vital to navigation errors. By the same consideration, this paper focuses on the relationship between navigation errors and the selecting pattern of three optical observation targets, namely Mars, Phobos and Deimos, but in the capture stage. Another significant issue affecting the integrated navigation errors of the Mars probe is the external measurements other than the optical observation. Recently, the range and its rate measurements at the line of sight between the Earth observation site and the Mars probe, which can be obtained by the well-known Doppler effects, have been extensively proved to be continuous and stable for the navigation purpose. Wu [37] combined both the optical observation in the cruise stage transmitted by the Mars probe and Doppler measurements provided by the Earth observation site to implement the orbit determination and propagation, which is also the primary task of the TT & C system. However, the two-way Doppler measurements above cannot be accepted by the autonomous navigation of the Mars probe for its too large time delay. Fortunately, the one-way Doppler measurements with no delays, only being transmitted from the Earth observation site to the Mars probe, can be well utilized to aid the optical observation to implement the autonomous navigation task. As for the one-way Doppler measurements, Zheng [38] proposed a passive measurement means with no a priori orbit parameters, by which the measurement errors are no more than 0.2 mm/s in the space tests. This space tests demonstrate promising prospects of one-way Doppler measurements in the autonomous navigation of the Mars probe in the capture stage.

This paper designs an integrated navigation scheme in the capture stage which comprises both the one-way Doppler measurements and optical observation for three targets in the Mars system.

2. Orbit dynamical models

After traveling into the capture stage, the probe is mainly affected by the force of the Mars' gravitation, the Sun's gravitation and the Mars' nonspherical perturbation. Because the time interval of this stage is relatively short, some smaller effects including the solar-radiation pressure, the Mars moon's gravitation and the higher-order nonspherical perturbation other than the J_2 items can be ignored.

The Mars' central gravitation is the main force in the capture stage. The dynamical formula is usually constructed in Mars-centered inertial system. Select J2000.0's Earth-equator plane as the coordinate system's X-Y plane. The dynamical formula is described as follows:

$$\ddot{\boldsymbol{r}} = -\frac{\mu_M}{r^3}\boldsymbol{r} + \mu_S\left(\frac{\boldsymbol{r}}{r^3} - \frac{\boldsymbol{r}_s}{r_s^3}\right) + \boldsymbol{a}_{ns} + \boldsymbol{a}_{\varepsilon} \qquad (1)$$

where μ_M denotes the gravitation constant of the Mars, μ_S denotes the gravitation constant of the Sun, $\boldsymbol{r}$ denotes the probe's position vector in the Mars-centered inertial system and r denotes the magnitude of the vector $\boldsymbol{r}$. The first part on the right side of (1) denotes the Mars' central gra-

vitation. The second part denotes the third-body gravitation from the Sun. The third part $\boldsymbol{a}_{ns}$ denotes the Mars' nonspherical perturbation. The fourth part $\boldsymbol{a}_{\varepsilon}$ denotes some other smaller perturbation. In the Mars-centered J2000.0 mean Mars-equator system, the Mars' nonspherical perturbation [39] is shown as follows:

$$\boldsymbol{a}_{ns}=\begin{pmatrix}\ddot{x}\\ \ddot{y}\\ \ddot{z}\end{pmatrix}_{ns}=\begin{pmatrix}\mu_M J_2\dfrac{x}{r^5}\left(7.5\left(\dfrac{z}{r}\right)^2-1.5\right)\\ \mu_M J_2\dfrac{y}{r^5}\left(7.5\left(\dfrac{z}{r}\right)^2-1.5\right)\\ \mu_M J_2\dfrac{z}{r^5}\left(7.5\left(\dfrac{z}{r}\right)^2-4.5\right)\end{pmatrix}. \tag{2}$$

In the navigation computation, $\boldsymbol{a}_{ns}$ needs to be transformed into the Mars-centered J2000.0 mean Earth-equator system.

3. Autonomous navigation measurement models

3.1 Measurement models of optical sensors

Theoretically, measurement models [40] of optical sensors can be regarded as pinhole imaging as Fig. 1 shows.

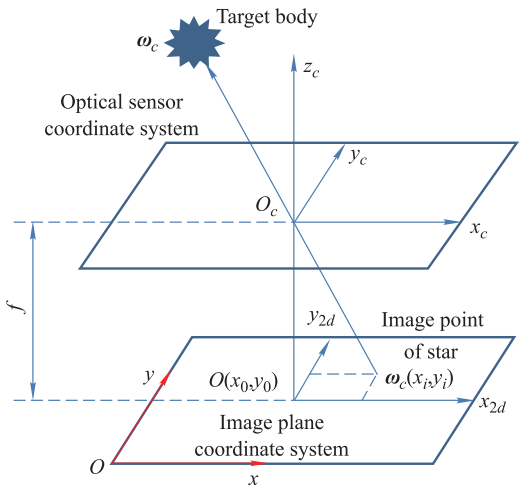

Fig. 1 Measurement model of optical navigation sensors

The imaging center coordinate of the target body is (x_i, y_i). The point of intersection between the main optical axis and the imaging plane is (x_0, y_0). The focus of the optical sensor is f. If the other imaging aberrance is not considered, the measurement vector of the target body in the sensor coordinate system is

$$\boldsymbol{\omega}_c=\frac{(x_i-x_0\quad y_i-y_0\quad z_i-z_0)^{\mathrm{T}}}{\sqrt{(x_i-x_0)^2+(y_i-y_0)^2+f^2}}. \tag{3}$$

Suppose the rotation matrix from the sensor coordinate system to the probe body coordinate system is $\boldsymbol{C}_c^b$. This matrix is mainly determined by the installation parameters of optical sensors on the probe. The rotation matrix from the probe body coordinate system to the probe-centered inertial coordinate system is $\boldsymbol{C}_b^i$. This rotation matrix is calculated by the attitude control system on board. Thus the insight orientation of the target body in the probe-centered inertial coordinate system is

$$\boldsymbol{\omega}_i=\boldsymbol{C}_c^i\boldsymbol{\omega}_c=\boldsymbol{C}_b^i\boldsymbol{C}_c^b\boldsymbol{\omega}_c=\frac{\boldsymbol{r}_T-\boldsymbol{r}}{\|\boldsymbol{r}_T-\boldsymbol{r}\|_2} \tag{4}$$

where $\boldsymbol{r}_T(x_T, y_T, z_T)$ denotes the position vector of the observation target and $\boldsymbol{r}(x, y, z)$ denotes the position vector of the Mars probe. They are both expressed in the Mars-centered J2000.0 mean Earth-equator system.

The partial derivation of observations with respect to the states of $\boldsymbol{r}$ and $\dot{\boldsymbol{r}}$ is

$$\frac{\partial \boldsymbol{w}_i}{\partial \boldsymbol{r}}=-R_T^{-\frac{3}{2}}\cdot$$

$$\begin{bmatrix}R-(x_T-x)^2 & (x_T-x)(y_T-y) & (z_T-z)(z_T-z)\\ (x_T-x)(y_T-y) & R-(y_T-y)^2 & (z_T-z)(y_T-y)\\ (x_T-x)(z_T-z) & (y_T-y)(z_T-z) & R-(z_T-z)^2\end{bmatrix}, \tag{5}$$

$$\frac{\partial \boldsymbol{w}_i}{\partial \dot{\boldsymbol{r}}}=\boldsymbol{0}_{3\times 3} \tag{6}$$

where $R_T=(x_T-x)^2+(y_T-y)^2+(z_T-z)^2$.

The sight vector of $\boldsymbol{w}_i$ from the Mars probe to the target body in the inertial system is the most significant measurement of optical sensors. The navigation filter selects this sight vector as the basic measurement. And the measurement errors of $\boldsymbol{w}_i$ are mainly determined by the position errors of the target's centroid in the image.

3.2 One-way Doppler measurement models

In the capture stage, the probe needs to be monitored in real-time by the Earth observation sites. Although the large delay which is consumed by the radio transmission is necessary, the continuous and stable radio signal can also be transmitted from some deep space observation station on the Earth. The Mars probe carries some specified clocks with high stability. After the Mars probe receives the radio signal from the Earth, the signal is then processed based on the known radar frequency and the one-way Doppler measurements. These measurements can be transformed into relative velocity between the Mars probe and the deep space observation station on the Earth.

The position of the deep space observation station in the Earth-centered fixed coordinate system is already known. It can be readily transformed into the Earth-centered J2000.0 mean Earth-equator system, and then into the Mars-centered J2000.0 mean Earth-equator system.

As the transmitting time is not given accurately, the time and the distance from the deep space observation station to the Mars probe at the corresponding instant should be calculated by some iterative scheme. Suppose the receive instant of the radio signal is t, the transmitting instant is $t-\Delta t$ but Δt is unknown, and the distance between the Mars probe and the deep observation station is R. The iterative calculating procedure is shown in Fig. 2.

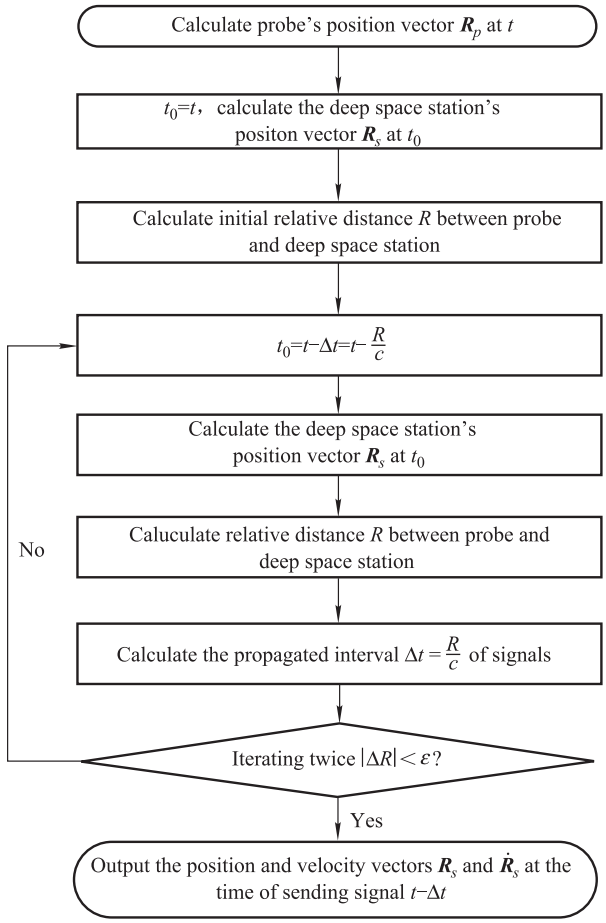

Fig. 2 Calculating iteratively the emitting instant of radio signals from the ground station

In the Mars-centered J2000.0 mean Earth-equator system, $\boldsymbol{r}(x,y,z)$ denotes the position vector when the Mars probe receives the radio signal, $\boldsymbol{r}_E(x,y,z)$ denotes the position vector when the deep space observation station sends the radio signal. Then the one-way Doppler measurement model is expressed as

$$v=\frac{(x-x_E)(\dot{x}-\dot{x}_E)+(y-y_E)(\dot{y}-\dot{y}_E)+(z-z_E)(\dot{z}-\dot{z}_E)}{\sqrt{(x-x_E)^2+(y-y_E)^2+(z-z_E)^2}}. \tag{7}$$

The partial derivations of observations with respect to the states $\boldsymbol{r}$ and $\dot{\boldsymbol{r}}$ are

$$\frac{\partial v}{\partial \boldsymbol{r}}=\begin{pmatrix} \dfrac{\dot{x}-\dot{x}_E}{\sqrt{(x-x_E)^2+(y-y_E)^2+(z-z_E)^2}}-\dfrac{(x-x_E)v}{(x-x_E)^2+(y-y_E)^2+(z-z_E)^2} \\ \dfrac{\dot{y}-\dot{y}_E}{\sqrt{(x-x_E)^2+(y-y_E)^2+(z-z_E)^2}}-\dfrac{(y-y_E)v}{(x-x_E)^2+(y-y_E)^2+(z-z_E)^2} \\ \dfrac{\dot{z}-\dot{z}_E}{\sqrt{(x-x_E)^2+(y-y_E)^2+(z-z_E)^2}}-\dfrac{(z-z_E)v}{(x-x_E)^2+(y-y_E)^2+(z-z_E)^2} \end{pmatrix}^{\mathrm{T}}, \tag{8}$$

$$\frac{\partial v}{\partial \dot{\boldsymbol{r}}}=\begin{pmatrix} \dfrac{x-x_E}{\sqrt{(x-x_E)^2+(y-y_E)^2+(z-z_E)^2}} \\ \dfrac{y-y_E}{\sqrt{(x-x_E)^2+(y-y_E)^2+(z-z_E)^2}} \\ \dfrac{z-z_E}{\sqrt{(x-x_E)^2+(y-y_E)^2+(z-z_E)^2}} \end{pmatrix}^{\mathrm{T}}. \tag{9}$$

4. Integrated navigation scheme combining optical and one-way Doppler measurements

In the capture stage, the target bodies include Mars, Phobos and Deimos. The designed autonomous navigation scheme which combines both the optical and the one-way Doppler measurements is shown in Fig. 3.

In the optical observation, Mars is treated as the plane target but Phobos and Deimos are treated as point targets. After obtaining the central pixels of Mars, Phobos and Deimos by some plane and point processing algorithms respectively, the high-precision sight orientation in the frame of optical sensors will be obtained hereby. According to the attitude parameters from the guidance, navigation and control (GNC) system on-board, the sight orientation is transformed from the sensor coordinate system into the probe-centered inertial coordinate system. The one-way Doppler measurements are continuous and stable which can be used in the navigation filter directly. Then the extended Kalman filter (EKF) algorithm can be conventionally used to calculate the position and velocity of the Mars probe. Additionally, the EKF calculation procedure in the autonomous navigation scheme is briefly described as follows [14].

The state and measurement equations are given as

$$\begin{cases} \ddot{\boldsymbol{x}}(\boldsymbol{r}(t),\dot{\boldsymbol{r}}(t))=f(\boldsymbol{x}(\boldsymbol{r}(t),\dot{\boldsymbol{r}}(t)))+\boldsymbol{\omega}(t) \\ \boldsymbol{y}(t)=h(\boldsymbol{x}(\boldsymbol{r}(t),\dot{\boldsymbol{r}}(t)))+\boldsymbol{\eta}(t) \end{cases} \tag{10}$$

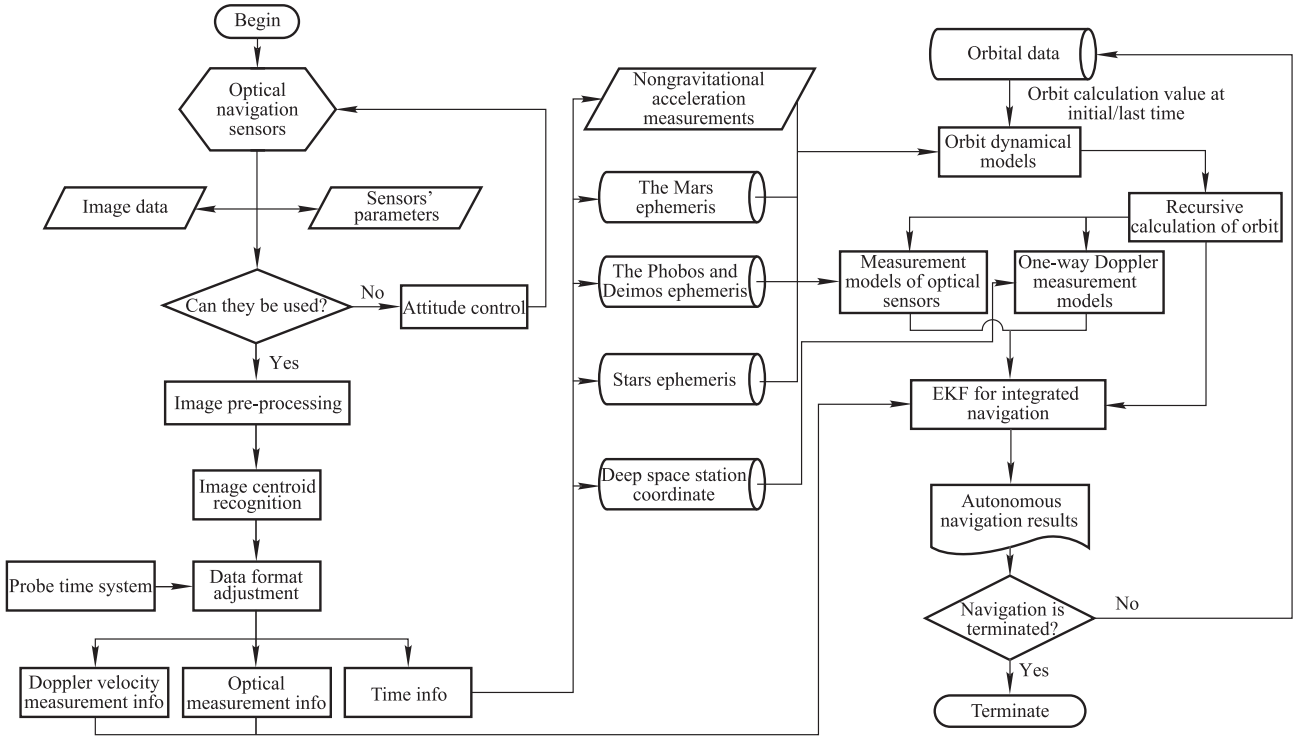

Fig. 3 Integrated navigation scheme utilizing both optical observation and one-way Doppler measurements

where $f(\cdot)$ denotes the state equation and $h(\cdot)$ denotes the measurement equation, $\boldsymbol{x}(\boldsymbol{r}(t),\dot{\boldsymbol{r}}(t))$ denotes the probe position and velocity, $\boldsymbol{y}(t)$ refers to the measurements including the optical observation of $\boldsymbol{w}_i$ and one-way Doppler observation of $\boldsymbol{\eta}(t)$, and $\boldsymbol{w}(t)$ and $\boldsymbol{\eta}(t)$ denote the procedure noise and measurement noise respectively.

The discretization equations can be described as follows:

$$\begin{cases}\boldsymbol{x}_{k+1}=\boldsymbol{\Phi}(t_{k+1},t_k)\boldsymbol{x}_k+\boldsymbol{\omega}_k\\ \boldsymbol{y}_{k+1}=\boldsymbol{H}_{k+1}\boldsymbol{x}_{k+1}+\boldsymbol{v}_{k+1}\end{cases}\tag{11}$$

where $\boldsymbol{\omega}_k$ and $\boldsymbol{v}_{k+1}$ denote the discretized procedure noise respectively, $\boldsymbol{H}_{k+1}$ denotes the discretized observation matrix, $\boldsymbol{\Phi}(t_{k+1},t_k)$ denotes the state transition matrix and can be approximately calculated by

$$\boldsymbol{\Phi}(t_{k+1},t_k)=\boldsymbol{I}_{6\times6}+\boldsymbol{F}_{k+1,k}(t_{k+1}-t_k)+\frac{1}{2}\boldsymbol{F}_{k+1,k}^2(t_{k+1}-t_k)^2\tag{12}$$

where $\boldsymbol{F}_{k+1,k}$ and $\boldsymbol{H}_{k+1}$ are respectively denoted by

$$\boldsymbol{F}_{k+1,k}=\frac{\partial\boldsymbol{f}(\boldsymbol{x}(t))}{\partial\boldsymbol{x}_{k+1,k}}=\frac{\partial(\dot{\boldsymbol{r}},\ddot{\boldsymbol{r}})}{\partial(\boldsymbol{r}_{k+1,k},\dot{\boldsymbol{r}}_{k+1,k})}=\begin{bmatrix}\boldsymbol{0}_{3\times3} & \boldsymbol{I}_{3\times3}\\ \dfrac{\partial\ddot{\boldsymbol{r}}}{\partial\boldsymbol{r}_{k+1,k}} & \dfrac{\partial\ddot{\boldsymbol{r}}}{\partial\dot{\boldsymbol{r}}_{k+1,k}}\end{bmatrix},\tag{13}$$

$$\boldsymbol{H}_{k+1}=\begin{bmatrix}\dfrac{\partial\boldsymbol{w}_i}{\partial\boldsymbol{r}} & \dfrac{\partial\boldsymbol{w}_i}{\partial\dot{\boldsymbol{r}}}\\ \dfrac{\partial v}{\partial\boldsymbol{r}} & \dfrac{\partial v}{\partial\dot{\boldsymbol{r}}}\end{bmatrix}.\tag{14}$$

According to the above dynamical and measurement equations, the basic EKF can be implemented as the following procedure.

Step 1 The predicted state of $\boldsymbol{x}_{k+1,k}$ is propagated from t_k to t_{k+1} by some numerical integration method.

Step 2 The predicted covariance matrix of $\boldsymbol{P}_{k+1,k}$ is propagated by

$$\boldsymbol{P}_{k+1,k}=\boldsymbol{\Phi}(t_{k+1},t_k)\boldsymbol{P}_k\boldsymbol{\Phi}^{\mathrm{T}}(t_{k+1},t_k)+\boldsymbol{\omega}_k.\tag{15}$$

Step 3 The Kalman gain matrix is calculated by

$$\boldsymbol{K}_{k+1}=\boldsymbol{P}_{k+1,k}\boldsymbol{H}_{k+1}^{\mathrm{T}}(\boldsymbol{H}_{k+1}\boldsymbol{P}_{k+1,k}\boldsymbol{H}_{k+1}^{\mathrm{T}}+\boldsymbol{V})^{-1}\tag{16}$$

where $\boldsymbol{V}$ denotes the covariance matrix of measurement noises.

Step 4 The state is updated by

$$\boldsymbol{x}_{k+1}=\boldsymbol{x}_{k+1,k}+\boldsymbol{K}_{k+1}(\boldsymbol{y}_{k+1}-\boldsymbol{H}_{k+1}\boldsymbol{x}_{k+1,k}).\tag{17}$$

Step 5 The covariance matrix is updated by

$$\boldsymbol{P}_{k+1}=(\boldsymbol{I}-\boldsymbol{K}_{k+1}\boldsymbol{H}_{k+1})\boldsymbol{P}_{k+1,k}.\tag{18}$$

5. Simulation test

5.1 Parameters setup

When the Mars probe is nearly into the capture stage, the initial epoch is set as 2020-01-01 12:00:0.000 (UTCG).

The true orbit of the Mars probe can be generated by the satellite tool kit (STK) software in the Mars-centered J2000.0 mean Earth-equator system. The flight procedure is set as three days wherein the capture stage is already included. The initial parameters are listed in Table 1. The true orbit of the Mars probe in the 3-day time span is described in Fig. 4 and Fig. 5.

Table 1 Initial state of the Mars probe

Direction	Position/m	Velocity/(m/s)
X	787 428 868.181	−2 902.862 031
Y	173 430 495.575	−657.767 255
Z	175 327 556.844	−624.561 085

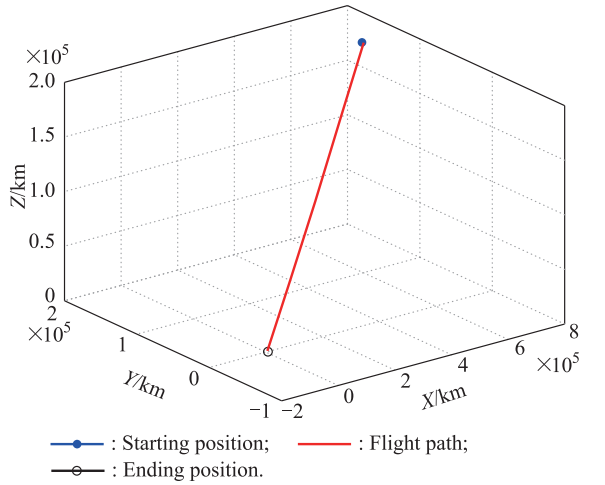

Fig. 4 Orbital position of the Mars probe in the whole flight procedure

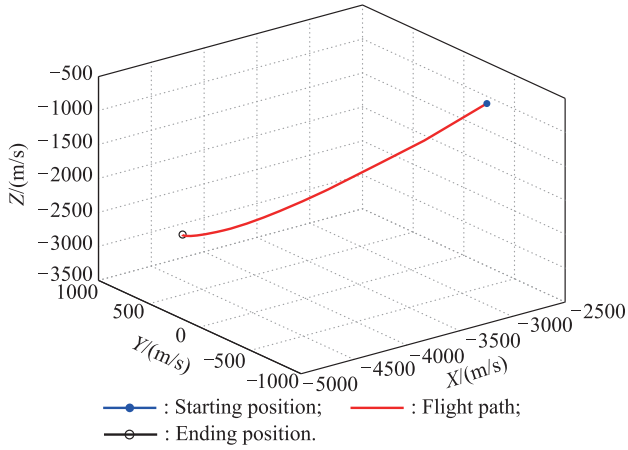

Fig. 5 Orbital velocity of the Mars probe in the whole flight procedure

According to Table 1, the initial position errors in X, Y, Z directions are given as 1 000 km and the initial covariance is given as 2 000 km respectively. The initial velocity errors in X, Y, Z directions are set as 5 m/s and the initial covariance is set as 10 m/s respectively.

In the Mars probe application, the general errors brought by the GNC system and image processing are usually at the magnitude of several tens of arc-seconds. Therefore, the biases and random errors of the optical observation are set as 10 and 100 arc-seconds respectively. The simulation step is set as 1 min. The target bodies include Mars, Phobos and Deimos.

In order to aid the Mars probe's optical observation, the deep space station on the Earth is given at 46.49° (latitude) and 130.78° (longitude). The one-way Doppler measurement period from the deep space station to the Mars probe is set as 10 s. The biases and random errors are both given as 0.005 m/s.

5.2 Optical measurement errors with 10 arc-seconds

(i) Selecting Phobos as the optical observing target

When the one-way Doppler measurements aid the optical observation, the position and velocity errors in the autonomous navigation are shown in Fig. 6.

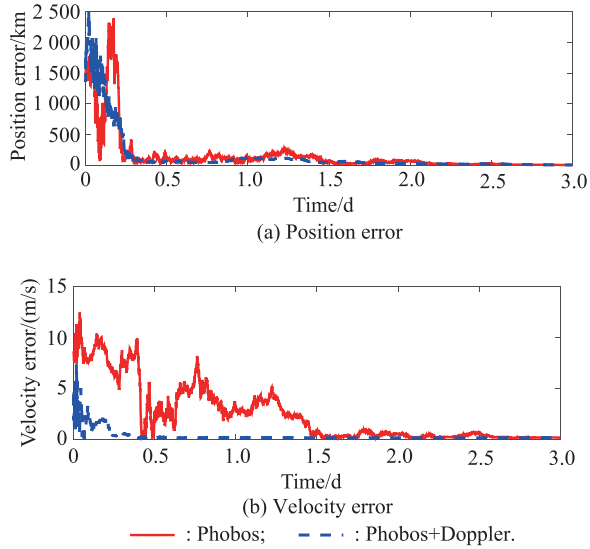

Fig. 6 Autonomous navigation errors in the Phobos-orientation optical observation mode (10 arc-seconds)

(ii) Selecting Deimos as the observing target

As the one-way Doppler measurements aid the optical observation, the position and velocity errors in the autonomous navigation is shown in Fig. 7.

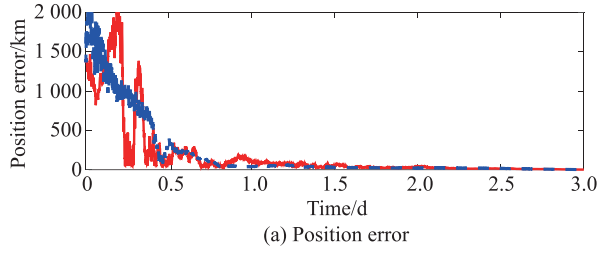

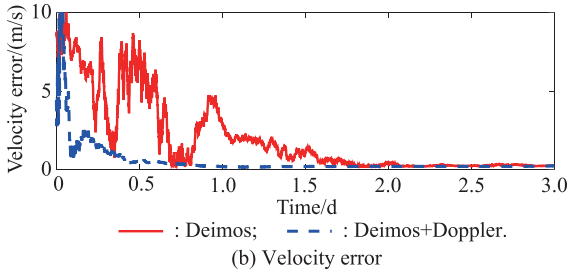

Fig. 7 Autonomous navigation errors in the Deimos-orientation optical observation mode (10 arc-seconds)

(iii) Selecting Mars as the observing target

As the one-way Doppler measurements aid the optical observation, the position and velocity errors in the autonomous navigation are shown in Fig. 8.

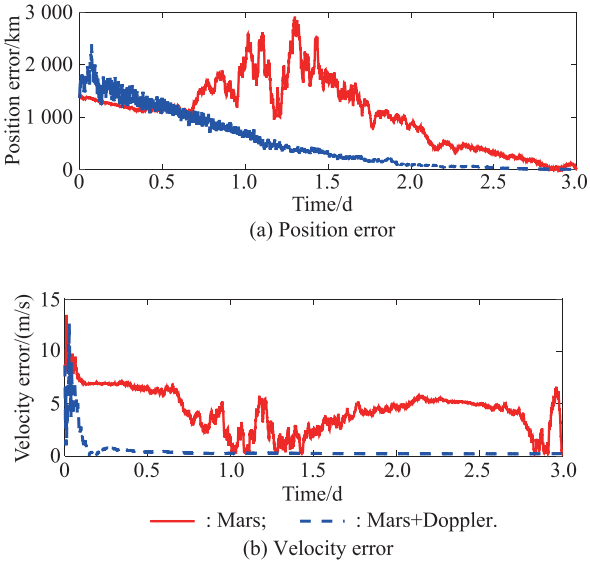

Fig. 8 Autonomous navigation errors in the Mars-orientation optical observation mode (10 arc-seconds)

5.3 Optical measurement errors with 100 arc-seconds

(i) Selecting Phobos as the observing target

As the one-way Doppler measurements aid the optical observation, the position and velocity errors in the autonomous navigation are shown in Fig. 9.

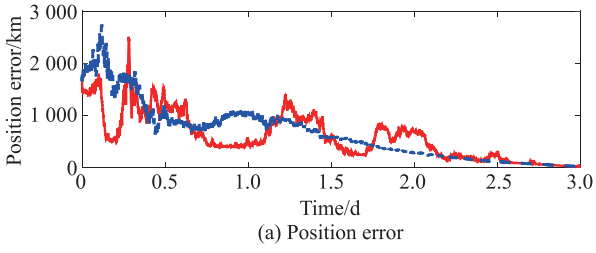

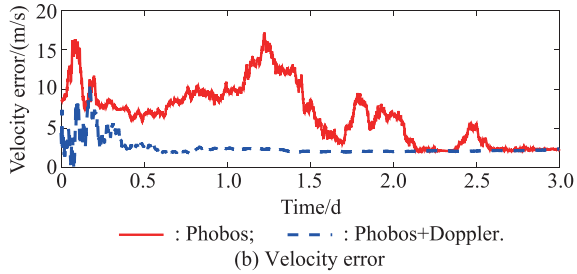

Fig. 9 Autonomous navigation errors in the Phobos-orientation optical observation mode (100 arc-seconds)

(ii) Selecting Deimos as the optical observing target

As the one-way Doppler measurements aid the optical observation, the position and velocity errors in the autonomous navigation are shown in Fig. 10.

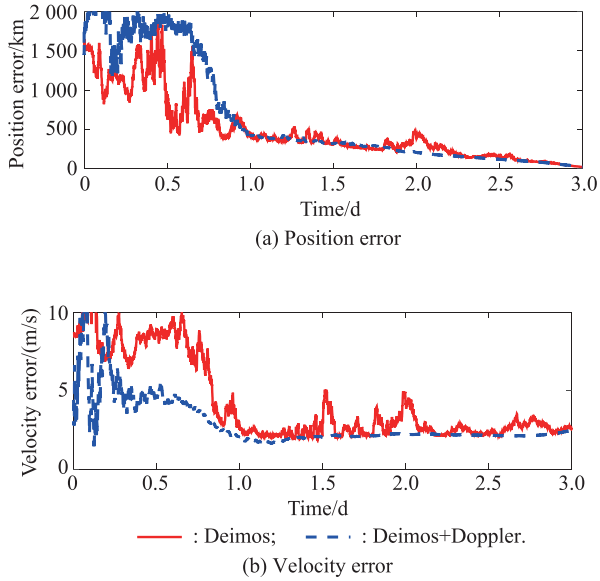

Fig. 10 Autonomous navigation errors in the Deimos-orientation optical observation mode (100 arc-seconds)

(iii) Selecting Mars as the optical observing target

As the one-way Doppler measurements aid the optical observation, the position and velocity errors in autonomous navigation are shown in Fig. 11.

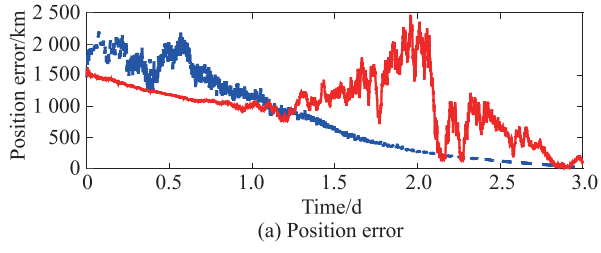

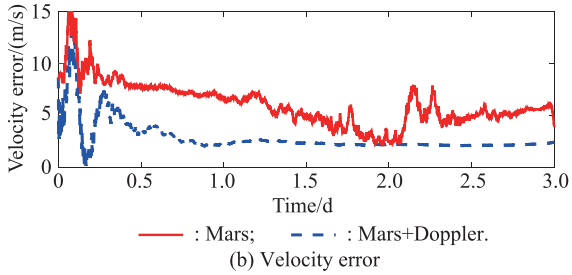

(b) Velocity error

Fig. 11 Autonomous navigation errors in the Mars-orientation optical observation mode (100 arc-seconds)

5.4 Analysis of navigation errors

Select the measurement interval from the 2.5th day to the 3rd day. Calculate the steady errors of the position and velocity according to the two cases of optical observation errors above. The navigation results are listed in Table 2 and Table 3.

According to Figs. 6 – 11 and Tables 2 – 3, some conclusions are drawn as follows.

Table 2 Autonomous navigation errors of Mars probe (the optical observation errors are set as 10 arc-seconds)

Observing target	Position error/km				Velocity error/(m/s)			
	Radial	Tangential	Normal	Total	Radial	Tangential	Normal	Total
Phobos	5.958	7.289	0.361	9.422	0.206	0.207	0.016	0.293
Phobos+Doppler	6.788	6.977	0.375	9.741	0.061	0.206	0.015	0.216
Deimos	4.369	7.819	1.171	9.033	0.201	0.195	0.009	0.281
Deimos+Doppler	6.683	7.359	0.863	9.978	0.061	0.211	0.007	0.219
Mars	175.992	7.193	0.434	176.139	3.876	0.651	0.017	3.931
Mars+Doppler	12.446	7.472	0.226	14.518	0.063	0.212	0.014	0.222

Table 3 Autonomous navigation errors of Mars probe (the optical observation errors are set as 100 arc-seconds)

Observing target	Position error/km				Velocity error/(m/s)			
	Radial	Tangential	Normal	Total	Radial	Tangential	Normal	Total
Phobos	53.074	72.416	3.864	89.865	1.448	2.102	0.144	2.557
Phobos+Doppler	22.104	70.888	3.504	74.337	0.665	2.073	0.181	2.184
Deimos	48.842	77.765	11.773	92.583	1.838	1.962	0.089	2.689
Deimos+Doppler	14.871	77.413	7.074	79.145	0.659	2.098	0.093	2.201
Mars	354.891	71.489	4.584	362.048	4.589	2.737	0.154	5.346
Mars+Doppler	27.948	74.137	2.915	79.284	0.663	2.097	0.124	2.203

(i) As the optical observation errors are given, the navigation errors are almost equivalent no matter whether Phobos or Deimos is selected as the optical observation. However, they are both better than Mars for the optical-alone navigation. This navigation superiority is due to the more rapid varying geometric relationship between the probe and Phobos or Deimos than that by choosing Mars as the optical observation.

(ii) The position errors of the integrated navigation, which both utilizes Phobos or Deimos optical observation and one-way Doppler measurements, are almost equivalent with that in the optical-alone navigation. However, the velocity errors, especially the radial components, in the whole-time span are obviously decreased in the integrated navigation.

(iii) The position and velocity errors of the integrated navigation with Mars optical observation and one-way Doppler measurements have been greatly reduced at a magnitude of dozens of times as compared with that in the optical-alone navigation.

(iv) In the framework of the integrated navigation wherein the optical observation is aided by one-way Doppler measurements, the position and velocity errors are almost comparative no matter which target is selected as the optical observation. In this sense, the integrated navigation errors do not depend on selecting the pattern of different optical observation targets.

6. Conclusions

Aimed at the high-precision and real-time requirements of the autonomous navigation in the capture stage, this paper proposes an integrated navigation scheme of the Mars probe. This scheme is mainly benefited from combing the one-target optical observation and one-way Doppler measurements from the observation site on Earth to the Mars probe. The simulation results show that observing the Mars moon has overwhelming superiority than Mars itself for the optical-alone navigation. Meanwhile, more precise velocity parameters can be obtained by the integrated navigation than that in the optical-alone observation case. Besides, the position errors can be greatly reduced in the integrated navigation as Mars is selected as the optical observation target. As is expected, the navigation errors are al-

most equivalent in three cases of the integrated navigation. In this regard, the designed integrated navigation scheme nearly eliminates the constraint that the navigation errors are subject to the selecting pattern of different targets in the optical-alone navigation case. From the numerical viewpoint, the position and velocity errors of the integrated navigation are less than 10 km and 0.3 m/s respectively, considering the 10 arc-seconds optical observation errors and several milimeter-per-second one-way Doppler measurement errors. As the optical observation errors are enlarged to 100 arc-seconds, the integrated navigation can also provide the position and velocity parameters which are still less than 100 km and 3.0 m/s respectively. Consequently, the proposed integrated navigation scheme can be abundantly utilized by the Mars probe in the capture stage.

However, some efforts are still needed to make to verify the advantage of the proposed integrated navigation scheme. On the one hand, the numerical observability is needed to be calculated to theoretically prove the simulation results. On the other hand, the integrated navigation scheme will be utilized and analyzed in the practical Mars probe flight experiments.

References

[1] GIPSMAN A, GUEHNAN M, KOGAN A. Autonomous navigation and guidance system for low thrust driven deep space missions. Acta Astronautica, 1999, 44(2): 353 – 364.

[2] WU W R, WANG D Y, NING X L, et al. Autonomous navigation principle and technology for deep space probe. Beijing: China Astronautic Publishing House, 2011. (in Chinese)

[3] NING X L, GUI M Z, FANG J C, et al. A novel differential Doppler measurement-aided autonomous celestial navigation method for spacecraft during approach phase. IEEE Trans. on Aerospace and Electronic Systems, 2017, 53(2): 587 – 597.

[4] MIGUEL A, MUNOZ B, IVAAN P. Framework for fast experimental testing of autonomous navigation algorithms. Applied Sciences, 2019, 9(7): 1997 – 2005.

[5] ZENG J J, QIN L, HU Y, et al. Integrating a path planner and an adaptive motion controller for navigation in dynamic environments. Applied Sciences, 2019, 9(7): 1384 – 1391.

[6] BHASKARAN S. Autonomous navigation for deep space missions. Spaceops, 2012, 10(2): 1 – 13.

[7] OWEN W M. Methods of optical navigation. Proc. of the 36th Conference on AIAA/AAS Spaceflight Mechanics, 2011: 211 – 215.

[8] LYNAM A E, KLOSTER K W, LONGUSKI J M. Multiple-satellite-aided capture trajectories at Jupiter using the Laplace resonance. Celestial Mechanics and Dynamical Astronomy, 2011, 109(1): 59 – 84.

[9] MAURETTE M. Mars rover autonomous navigation. Autonomous Robots, 2003, 14(2): 199 – 208.

[10] KOHLHASE C E. Autonomous navigation preparation for future unmanned space mission. Journal of Navigation, 1975, 22(1): 16 – 34.

[11] NING X L, LI Z, YANG Y Q, et al. Analysis of Ephemeris errors in autonomous celestial navigation during Mars approach phase. Journal of Navigation, 2017, 70(3): 505 – 526.

[12] RONG J, XU L P, ZHANG H, et al. Augmentation method of XPNAV in Mars orbit based on Phobos and Dermos observations. Advances in Space Research, 2016, 58(9): 1864 – 1878.

[13] JERATH N, OHTAKAY H. Mariner IX optical navigation using Mars lit limb. Journal of Spacecraft, 2012, 11(7): 505 – 511.

[14] MA P B, JIANG F H, BAOYIN H X. Autonomous navigation of Mars probes by combining optical data of viewing Martian Moons and SST data. Journal of Navigation, 2015, 68(6): 1019 – 1040.

[15] YAN H T, DAI Z, HU Y P, et al. Optical measurement aided autonomous navigation for pinpoint Mars landing. Optik, 2018, 157: 976 – 987.

[16] MA P B, WANG T S, JIANG F H, et al. Autonomous navigation of Mars probes by single X-ray pulsar measurement and optical data of viewing Martian moons. Journal of Navigation, 2016, 70(1): 18 – 32.

[17] ACTON C H. Processing onboard optical data for planetary approach navigation. Journal of Spacecraft and Rockets, 2012, 9(10): 746 – 750.

[18] HUANG X Y, CUI H T, CUI P Y. An autonomous optical navigation and guidance for soft landing on asteroids. Acta Astronautica, 2004, 54(10): 763 – 771.

[19] LOWMAN A E, STAUDER J L. Stray light lessons learned from the Mars reconnaissance orbiter's optical navigation camera. Proc. of the Conference on the SPIE and Location, 2004: 1123 – 1130.

[20] ELACHI C. The critical role of communications and navigation technologies to the success of space science enterprise missions. Proc. of the Keynote Address Descanso International Symposium, 1999: 3263 – 3269.

[21] RIEDEL J E, BHASKARAN S, DESAI S. Autonomous optical navigation (AutoNav) DS 1 technology validation report. Pasadena: Jet Propulsion Laboratory, 2000.

[22] ANTREASIAN P G, BAIRD D T, BORDER J S. 2001 Mars Odyssey orbit determination during interplanetary cruise. Journal of Spacecraft and Rockets, 2005, 42(3): 394 – 405.

[23] LIU J, MA J, TIAN J W, et al. X-ray pulsar navigation method for spacecraft with pulsar direction error. Advances in Space Research, 2010, 46(11): 1409 – 1417.

[24] WANG Y D, ZHENG W, SUN S M, et al. X-ray pulsar – based navigation using time-differenced measurement. Aerospace Science and Technology, 2014, 36(3): 27 – 35.

[25] WANG Y D, ZHENG W, SUN S M, et al. X-ray pulsar-based navigation system with the errors in the planetary ephemerides for Earth-orbiting satellite. Advances in Space Research, 2013, 51(12): 2394 – 2404.

[26] EASTON R L, BUISSON J A. The contribution of navigation technology satellite to the global positioning system. Journal of Neurophysiology, 1979, 107(7): 1881 – 1889.

[27] WEI W H, GAO Z H, GAO S S, et al. A SINS/SRS/GNS autonomous integrated navigation system based on spectral redshift velocity measurements. Sensors, 2018, 18(4): 1145 – 1152.

[28] NING X L, WANG L H, BAI X B, et al. Autonomous satellite navigation using starlight refraction angle measurements. Advances in Space Research, 2013, 51(9): 1761 – 1772.

[29] WHITE R L, THURMAN S W, BARNES F A. Autonomous satellite navigation using observations of starlight atmospheric refraction. Journal of Navigation, 1985, 32(4): 317 – 333.

[30] WANG H Y, GAO Z Q, WANG T F, et al. Study on command attitude law for refracted starlight observation in SINS/RCNS integrated navigation. Advances in Space Research, 2018, 62(3): 721 – 731.

[31] WANG X L, WANG B, LI H N. An autonomous navigation scheme based on geomagnetic and starlight for small satellite. Acta Astronautica, 2012, 81(3): 40 – 50.
[32] MORTARI D, CONWAY D. Single-point position estimation in interplanetary trajectories using star trackers. Celestial Mechanics and Dynamical Astronomy, 2017, 128(1): 115 – 130.
[33] LIU J, FANG J C, MA X, et al. X-ray pulsar/starlight Doppler integrated navigation for formation flight with ephemerides errors. IEEE Aerospace and Electronic Systems Magazine, 2015, 30(3): 30 – 39.
[34] LIU R X, ZHAN J Q. Research on autonomous navigation algorithms for the Mars probe via speed and angle measurement sensors. Journal of Deep Space Exploration, 2016, 3(3): 219 – 224. (in Chinese)
[35] MING X, WANG X L, LI Q S. Autonomous celestial navigation scheme design for Mars probe's capture phase. Aero Weaponry, 2017, 30(3): 41 – 46. (in Chinese)
[36] ZHANG X W, WANG D Y, HUANG X Y. Study on the selection of the beacon asteroids in autonomous optical navigation for interplanetary exploration. Journal of Astronautics, 2009, 30(3): 947 – 952. (in Chinese)
[37] WU G Y, YANG Y, WANG X J, et al. To improve orbit determination and prediction accuracy for Mars probe with optical measurement during cruise phase. Journal of Astronautics, 2014, 35(2): 151 – 156. (in Chinese)
[38] ZHENG W M, MA M L, WANG W B. High-precision passive Doppler measurement method and its application in deep space explorer. Journal of Astronautics, 2013, 34(11): 1462 – 1467. (in Chinese)
[39] VALLADO D A. Fundamentals of astrodynamics and applications. Chicago: Donnelley and Sons Company, 1997.
[40] KAEHLER A, BRADSKI G. Learning OpenCV 3: computer vision in C++ with the OpenCV Library. Boston: O'Reilly Media, Inc, 2016.

Biographies

ZHANG Zhibin was born in 1975. He received his B.S. degree from Peking University in 1997 and M.E. degree in 2013 from University of Science and Technology of China, respectively. He is currently pursuing his Ph.D. degree at University of Science and Technology of China. He is now a professor at State Key Laboratory of Astronautics Dynamics. His research interests include navigation guidance and control of spacecraft.
E-mail: BrownPKU@aliyun.com

JI Haibo was born in 1964. He received his B.S. degree from Zhejiang University in 1984 and Ph.D. degree in 1990 from Peking University, respectively. He is now a professor at University of Science and Technology of China. His research interests include nonlinear systems and control, and guidance and control of aerial vehicles.
E-mail: jihb@ustc.edu.cn

YANG Jie was born in 1985. He received his B.S. and Ph.D. degrees in navigation, guidance and control from National University of Defense Technology in 2007 and 2013 respectively. From 2013 to 2019, he was with the State Key Laboratory of Astronautic Dynamics as a research assistant. His research interests include the spacecraft orbit determination, multi-target tracking and identification, and inertial-based integrated navigation.
E-mail: nudtyang@163.com